

ORIGINAL
RESEARCH

S.J. Price
R. Jena
N.G. Burnet
P.J. Hutchinson
A.F. Dean
A. Peña
J.D. Pickard
T.A. Carpenter
J.H. Gillard

Improved Delineation of Glioma Margins and Regions of Infiltration with the Use of Diffusion Tensor Imaging: An Image-Guided Biopsy Study

BACKGROUND AND PURPOSE: The efficacy of radiation therapy, the mainstay of treatment for malignant gliomas, is limited by our inability to accurately determine tumor margins. As a result, despite recent advances, the prognosis remains appalling. Because gliomas preferentially infiltrate along white matter tracks, methods that show white matter disruption should improve this delineation. In this study, results of histologic examination from samples obtained from image-guided brain biopsies were correlated with diffusion tensor images.

METHODS: Twenty patients requiring image-guided biopsies for presumed gliomas were imaged preoperatively. Patients underwent image-guided biopsies with multiple biopsies taken along a single track that went into normal-appearing brain. Regions of interest were determined from the sites of the biopsies, and diffusion tensor imaging findings were compared with glioma histology.

RESULTS: Using diffusion tissue signatures, it was possible to differentiate gross tumor (reduction of the anisotropic component, $q > 12\%$ from contralateral region), from tumor infiltration (increase in the isotropic component, $p > 10\%$ from contralateral region). This technique has a sensitivity of 98% and specificity of 81%. T2-weighted abnormalities failed to identify the margin in half of all specimens.

CONCLUSION: Diffusion tensor imaging can better delineate the tumor margin in gliomas. Such techniques can improve the delineation of the radiation therapy target volume for gliomas and potentially can direct local therapies for tumor infiltration.

Gliomas are the most common primary brain tumors. Their pattern of rapid, infiltrative growth means that conventional treatments usually fail to provide a cure. Despite great improvements in our understanding of the biology of gliomas, little impact has been made on the appalling prognosis of these tumors. Attempts at developing glioma-specific therapies have so far failed to provide therapeutic options that improve outcome. There is a need, therefore, to further improve existing treatments.

Radiation therapy remains the main nonsurgical treatment for gliomas. It is well established that radiation therapy prolongs life and delays recurrence in high-grade gliomas,¹ yet virtually all patients still develop recurrent tumor within the treated volume.^{2,3} Very high doses of radiation therapy (up to 90 Gy) may sterilize tumors, but the incidence of radiation necrosis is considered unacceptably high.⁴ Gliomas have a propensity for infiltration, especially along white matter tracks, where glioma cells can be identified considerable distances away from the edge of gross tumor.^{5,6} Because neither CT⁷⁻¹⁰ nor MR imaging¹¹⁻¹³ can accurately localize microscopic glioma infiltration, radiation therapy planning includes a margin to account for this occult spread. As a rule, this mar-

gin is applied uniformly in all directions, and in all patients. Because normal brain is sensitive to radiation therapy, the dose given has to be limited to prevent radiation necrosis. A better definition of the tumor margin should allow a higher dose to be delivered to a smaller region of the brain with improved tumor control and less risk of radiation necrosis using modern conformal radiation therapy techniques.

It is well recognized that glioma cells preferentially infiltrate along white matter tracks.^{5,6} Diffusion tensor imaging (DTI) is an MR technique that is sensitive to the directional diffusion of water along white matter tracks.¹⁴ Studies have shown that DTI reveals larger peritumoral abnormalities in gliomas that are not apparent on conventional MR imaging, a feature that is absent with minimally or noninfiltrative tumors such as metastases or meningiomas.^{15,16} These abnormalities seem to precede the development of gross tumor recurrence on follow-up imaging.¹⁷

Whether these DTI changes are due to tumor infiltration or other reactive changes caused by the tumor remains unknown. In this study, we aim to determine whether DTI changes allow the identification of regions of tumor infiltration that cannot be seen on conventional imaging by comparing these changes to results from histologic examinations performed on tissue obtained from image-guided biopsies. Where possible, biopsies have been targeted from areas of normal imaging close to the tumor to address the specificity of the technique.

Methods

Patients. The study group comprised 20 patients who required an image-guided biopsy for a presumed glioma. The patient details are summarized in Table 1. All patients gave informed consent, and the study was approved by the Local Research Ethics Committee.

Imaging Studies. Patients were imaged approximately 48 hours before tumor biopsy using a 3T Bruker MedSPEC S300 MR (Bruker Biospin, Ettlingen, Germany). All patients were imaged in the axial plane

Received November 10, 2005; accepted after revision December 22.

From the Academic Neurosurgical Unit (S.J.P., P.J.H., A.P., J.D.P.) and Wolfson Brain Imaging Centre (S.J.P., J.D.P., T.A.C.), Department of Clinical Neurosciences, University Department of Radiology (S.J.P., A.P., J.H.G.), University Department of Oncology (R.J., N.G.B.), and Department of Neuropathology (A.F.D.), University of Cambridge and Cambridge University Hospitals NHS Foundation Trust, Addenbrooke's Hospital, Cambridge, United Kingdom.

This study was funded by the New and Emerging Applications of Technology Programme from the Department of Health, UK. R.J. was supported by an unrestricted educational grant from Siemens Oncology Care Systems. P.J.H. is supported by an Academy of Medical Sciences/Health Foundation Senior Surgical Scientist Fellowship.

Address correspondence to Stephen J. Price, Academic Neurosurgery Unit, Box 167, Addenbrooke's Hospital, Cambridge, CB2 2QQ, United Kingdom; e-mail: sjp58@cam.ac.uk

Patient details			
Patient No./ Age (y)/Sex	WHO Grade	Histology	Biopsy into Histologically Normal Brain
1/41/M	II	Astrocytoma	No
2/45/M	II	Astrocytoma	Yes
3/33/M	II	Astrocytoma	Yes
4/39/F	II	Oligodendroglioma	Yes
5/44/M	II	Oligodendroglioma	Yes
6/42/M	II	Oligodendroglioma	No*
7/61/F	II	Oligodendroglioma	No
8/18/M	II	Oligodendroglioma	Yes
9/41/M	III	Anaplastic oligoastrocytoma	No
10/67/M	III	Anaplastic oligoastrocytoma	Yes
11/66/F	III	Anaplastic oligoastrocytoma	Yes
12/64/M	III	Anaplastic oligoastrocytoma	No
13/51/M	IV	Glioblastoma	No
14/75/M	IV	Glioblastoma	No
15/31/M	IV	Glioblastoma	Yes
16/60/M	IV	Glioblastoma	Yes
17/54/F	IV	Glioblastoma	No*
18/72/M	IV	Glioblastoma	No
19/78/M	IV	Glioblastoma	No
20/22/M	IV	Supratentorial PNET	No

Note:—PNET indicates primitive neuroectodermal tumor.

* Biopsies in these patients were not taken into normal brain due to hemorrhage.

with 4-mm section thickness and a 1-mm intersection separation. The imaging protocol included a dual-echo T2/proton density fast spin-echo sequence (repetition time [TR], 6275 ms; echo time [TE], 120 ms/20 ms; field of view [FOV], 16.8 × 35.8 cm²; matrix, 256 × 512; 27 sections), an inversion recovery T1-weighted sequence (TR, 3650 ms; TE, 45.2 ms; TI, 593.7 ms; FOV, 19.2 × 25.6 cm²; matrix, 512 × 512; 19 sections) performed after the administration of 0.1 mmol/kg gadoteridol (ProHance; Bracco Diagnostics, Princeton, NJ) and a single-shot, spin-echo, echo-planar imaging diffusion tensor sequence (TR, 6000 ms; TE, 100 ms; FOV, 20 × 20 cm²; matrix, 100 × 100 interpolated to 128 × 128 for reconstruction; 27 sections). Each section from the DTI sequence was collected from 12 noncolinear gradient directions. For each direction, 1 T2 (*b*₀) image and 5 diffusion gradient-weighted images were collected (with *b* values of 318, 392.5, 785, 1177.5, and 1570 s/mm²).

Image-Guided Biopsy Technique. All patients were biopsied under general anesthesia. For the first 5 patients, we used an MR-guided frame-based stereotactic biopsy technique described previously by Donovan et al.¹⁸ An MR-compatible stereotactic Leksell G frame (Elekta Instruments, Stockholm, Sweden) was fixed to the patient's head under general anesthesia, and the patient was imaged at 3T using a 3D echo-spoiled gradient recalled (SPGR) echo sequence (TR, 20 ms; TE, 5 ms; flip angle, 20°; FOV, 25.6 × 25.6 × 25.6 cm³; matrix, 256 × 256 × 128; 128 sections; spatial resolution, 1 × 1 × 2 mm). The target was identified and the coordinates selected by first determining the center of the frame and then measuring the lateral and anteroposterior distances to the target from the center. Biopsies were taken with the use of a 10 × 2-mm side-cutting biopsy needle and were taken from the center of the target then at 1-cm intervals along a single needle-track back into what was considered normal-appearing brain on the basis of biopsy core appearance and conventional MR imaging. The lateral and anteroposterior angles of the biopsy trajectory were recorded and used to calculate the coordinates of the biopsy sites at 1-cm intervals along the track. Regions of interest (ROIs) from each site measuring 10 × 4 mm (the approximate volume of tissue sampled) were used for subsequent analysis.

The subsequent 15 patients underwent a frameless image-guided biopsy. This change was largely due to a software upgrade that allowed us to import the enhanced 3D SPGR sequence into our neuronavigation system (StealthStation Treon; Medtronic Navigation, Minneapolis, Minn). Patients were imaged using a contrast-enhanced 3D SPGR sequence (TR, 19.18 ms; TE, 5 ms; FOV, 18.0 × 22.0 × 25.6 cm³; matrix, 180 × 220 × 256, interpolated to 256 × 256 × 256 for reconstruction; 256 sections; spatial resolution, 0.7 × 0.86 × 1 mm). Image registration was performed using multitechnique radiographic scalp markers (IZI Medical Products, Baltimore, Md). Biopsies were performed with the use of a side-cutting, 10 × 2-mm Medtronic image-guided biopsy needle and again were taken from the selected target and at 1-cm intervals back into apparently normal brain. Coordinates from each biopsy site were recorded and again used for subsequent analysis. Postoperative imaging confirmed accuracy of biopsies to be within 3 mm of the selected target.

Image Processing and Data Analysis. Processing of the diffusion tensor data set was performed using an in-house program implemented in Matlab (MathWorks, Natick, Mass), following the method proposed by Basser et al.¹⁹ For each voxel, the eigenvalues ($\lambda_1, \lambda_2, \lambda_3$) are computed and then used to calculate fractional anisotropy (FA) as well as the isotropic component of diffusion, *p*, and the anisotropic component of diffusion, *q*, using the following equations²⁰:

$$1) \quad FA = \sqrt{\frac{3}{2}} \frac{\sqrt{(\lambda_1 - D)^2 + (\lambda_2 - D)^2 + (\lambda_3 - D)^2}}{\sqrt{\lambda_1^2 + \lambda_2^2 + \lambda_3^2}}$$

$$2) \quad p = \sqrt{3D}$$

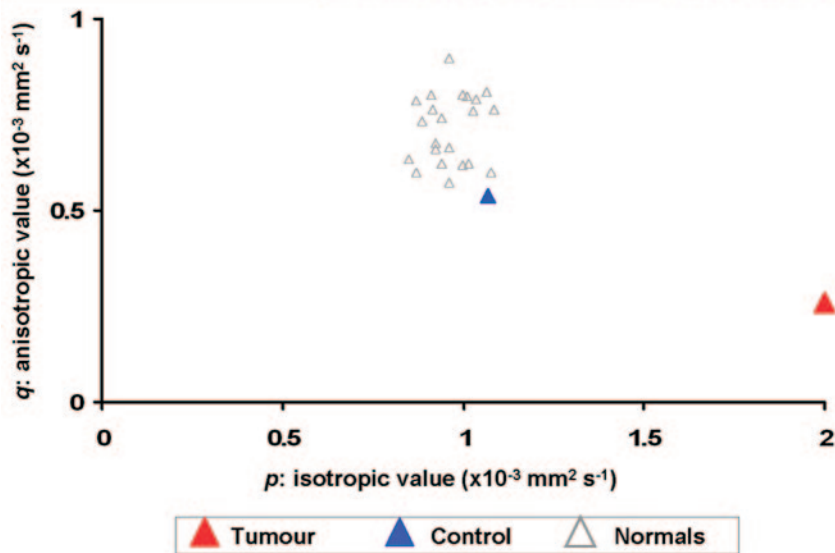
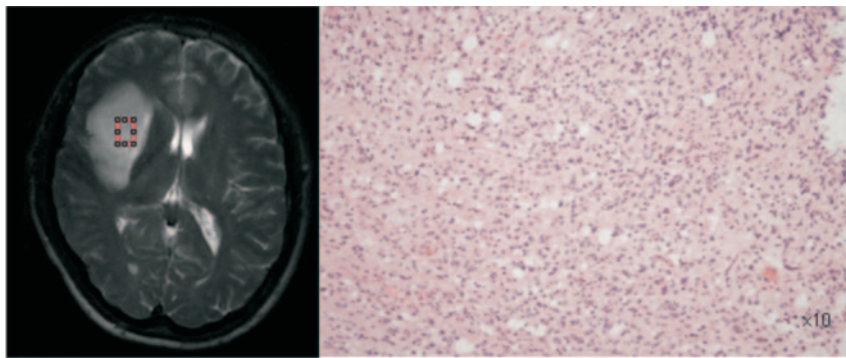
$$3) \quad q = \sqrt{(\lambda_1 - D)^2 + (\lambda_2 - D)^2 + (\lambda_3 - D)^2}$$

Where *D* is the mean diffusivity:

$$4) \quad D = \frac{\lambda_1 + \lambda_2 + \lambda_3}{3}$$

These parameters were calculated on a voxel-by-voxel basis to produce maps of *p*, *q*, and FA. These maps, as well as the T2-weighted and enhanced inversion-recovery T1-weighted images, were coregistered to the SPGR used for biopsy planning using vtkCSIG (Computational Imaging Sciences Group, King's College, London).²¹ At each ROI, measures of *p*, *q*, and FA were made, and the appearance on T2- and enhanced T1-weighted imaging was noted. Measures of diffusion tensor parameters were all normalized to ROIs from a similar anatomic location in the contralateral hemisphere and expressed as a ratio to normal brain.

Analysis of Biopsy Material. At least 2 biopsies were obtained per location. A 0.5-mm section from the end of the biopsy core was removed for an intraoperative smear before the biopsies were fixed in 30% formal saline for 1–3 days, processed for paraffin embedding, sectioned at 5- μ m thickness, and stained with hematoxylin/eosin. Immunocytochemical staining was performed with antibodies directed against Ki67 (monoclonal, MIB1 antibody [Dako Denmark, Glostrup, Denmark]; 1/300 dilution; 3-minute high-power microwave pretreatment), glial fibrillary acidic protein (polyclonal [Dako UK, Ely, Cambridgeshire, UK]; 1/400 dilution), synaptophysin (monoclonal [Vector Laboratories, Peterborough, UK]; 1/30 dilution; 3-minute pressure-cooking pretreatment), and NeuN (monoclonal [Chemicon International, Temecula, Calif]; 1/100 dilution; 3-minute high-power microwave pretreatment). MIB1 and NeuN sections were pretreated by microwave at high power in buffer. Synaptophysin sections were pressure-cooked for 3 minutes. Negative controls comprised omission of the primary antiserum. Positive controls were brain tissue and, for MIB1, tonsil. Visualization was achieved using an avidin-biotin complex kit (Dako) and diaminobenzidine as chromogen. Biopsy specimens were examined by an experienced



neuropathologist who was blinded to imaging findings and were broadly classified into 3 groups: those that had only tumor with no normal-appearing brain tissue in the biopsy, those that demonstrated normal brain infiltrated with tumor, and those that had normal-appearing brain. Tumors were graded according to WHO 2000 criteria. Histologic examination findings were compared with imaging findings.

Statistical Analysis. All results are quoted as mean \pm SEM. Statistical significance was assessed using unpaired *t* tests (SPSS for Windows release 11.5.0; SPSS, Chicago, Ill).

Results

Tumor Biopsies. In total, 77 ROIs were biopsied in 20 patients (mean age, 50.7 years; range, 18.4–78.9; 4 women). The median number of biopsies per patient was 4 (range, 2–6). In 2 patients (patients 6 and 17), biopsies were abandoned after the second region because of hemorrhage. In both cases, the patients woke without neurologic deficit, and postoperative imaging revealed a small hematoma at the biopsy site. The final histologic diagnoses (summarized in Table 1) were 8 WHO grade II gliomas (3 astrocytomas and 5 oligodendrogliomas), 4 WHO grade III gliomas (all anaplastic oligoastrocytomas), and 8 WHO grade IV tumors (7 glioblastomas and 1 supratentorial primitive neuroectodermal tumor [PNET]). The biopsy regions found 43 showing gross tumor, 20 that had normal-appearing white matter infiltrated with tumor cells, and 14 normal regions.

Histologic Correlation

Conventional MR Imaging Methods. In 18 patients in whom the biopsy trajectories were taken into normal-appear-

Fig 1. An example of the biopsy findings from a region of tumor in a 41-year-old man who presented with seizures and a mild left hemiparesis. The T2-weighted image shows that the biopsy was taken from the center of the lesion and that histologic examination (*above right*) confirmed it as a WHO grade III anaplastic oligoastrocytoma. The tissue signature from this region shows significant increase in *p* (10% compared with normal side) with a significant decrease in *q* (12%).

ing peritumoral areas (ie, normal T2 signal intensity and outside areas of gadolinium enhancement on T1-weighted images), histologic examination revealed the presence of tumor in 8 of 18 regions. Occult tumor was seen more commonly in the WHO grade IV tumors (identified in 5 of 7 samples) than the WHO grade III (seen in 2 of 4 patients) or WHO grade II gliomas (seen in 1 of 7 patients).

Diffusion Tensor Tissue Signatures.

The findings from the tissue signatures were as described previously.²⁰ In regions of gross tumor, there was a marked increase in *p*, the isotropic component of the diffusion tensor, (1.36 ± 0.71) and a marked decrease in *q*, the anisotropic component of the diffusion tensor, (0.62 ± 0.04). An example is shown in Fig 1. Areas of tumor infiltration had an increase in *p* (1.32 ± 0.05) but a marginally increased *q* ($1.18 \pm$

0.09). An example of the findings in infiltration is shown in Fig 2. Both *p* and *q* were similar to the contralateral side in regions of normal brain (ratios to normal, contralateral side were $p = 1.02 \pm 0.02$ and $q = 1.12 \pm 0.06$) (an example is shown in Fig 3). A threshold was determined that could, with the use of previously published data, differentiate between these regions.²⁰ Areas with tumor had a reduced *q* value that was more than 12% lower than the normal side (which was independent of the *p* value), whereas infiltrated regions had a *p* value that was more than 10% higher than the normal side (and a *q* value that was either slightly higher or less than 12% lower than the abnormal side). Using these thresholds, tissue signatures could correctly detect 42 of 43 areas of gross tumor. The single case in which gross tumor was not detected was within a region of heavy calcification within the center of a supratentorial PNET. Both T2- and gadolinium-enhanced T1-weighted images missed 1 region of gross tumor. In the infiltrating tumor region, enhanced T1-weighted imaging could identify only 11 of 20 regions and T2-weighted could identify 12 of 20. The tissue signatures correctly identified these areas in 19 of 20 ROIs. One false-positive result was obtained using the diffusion tensor tissue signature technique. In this biopsy, the tissue signature was of tumor infiltration, but histologic analysis revealed a marked polymorphonuclear infiltrate with no evidence of tumor. Using these values, the overall sensitivity was 98% and specificity was 81%.

Fractional Anisotropy. The normalized FA values for the tumor were significantly lower than infiltrated regions (0.6 ± 0.06 versus 0.86 ± 0.12 ; $P = .02$) or normal brain (0.6 ± 0.06 versus 0.97 ± 0.06 ; $P < .001$). There was, however, no significant differ-

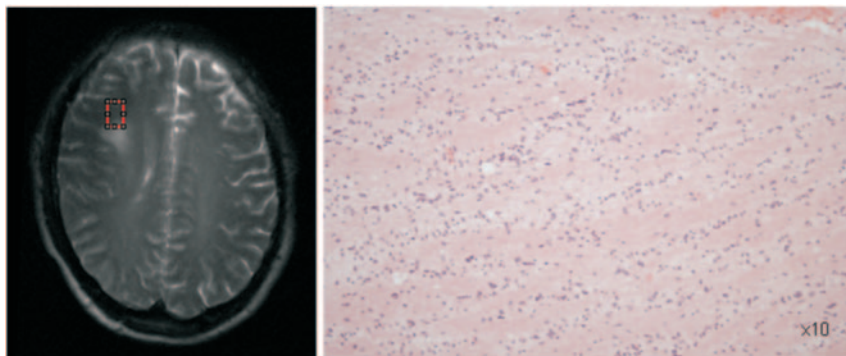
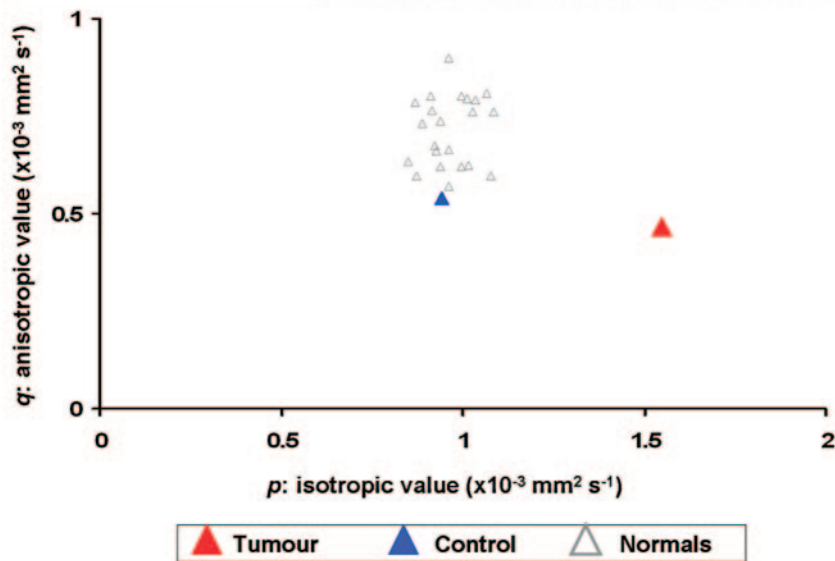


Fig 2. Biopsy from a region 2.5 cm from the target of Fig 1. The T2-weighted image shows it has been taken from a region that is apparently normal. Histologic examination, however, confirms normal white matter with tumor infiltration. The tissue signature in this region shows a significant increase in p without much change in q .



ence in FA values between the infiltrated regions and normal brain ($P = .27$). There was such overlap in the values of FA among the 3 regions that thresholds could not be determined.

Discussion

This study has shown that the abnormalities seen in the peritumoral region of gliomas when using diffusion tensor MR imaging are due to tumor infiltration. Furthermore, this study shows that this technique can define 2 regions around gliomas—an area with a decrease in the anisotropic component of the diffusion tensor tissue signature (q) more than our threshold of 12% that signifies the gross tumor and a region with normal q and an increase in the isotropic component, p , of greater than 10% of the normal side that signifies an area of tumor infiltration into normal brain. An example of such regions plotted on a gadolinium-enhanced T1-weighted image of a glioblastoma is shown in Fig 4.

Previous studies have shown that conventional MR imaging sequences cannot accurately identify tumor margins.¹¹⁻¹³ Our study has shown that tumor infiltration occurs in brain that appears normal on T2-weighted images in 40% of cases. This figure is similar to those reported by others. Lunsford et al¹¹ found that tumors extended into regions of normal T2 signal intensity in all cases of glioblastoma, in one third of anaplastic astrocytomas, and in one sixth of low-grade astrocytomas. Kelly et al¹² performed serial image-guided biopsies in patients with gliomas, and in the 8 biopsies taken from areas with normal T2 signal intensity, he could identify infiltrating

techniques, however, are currently limited by the relatively poor resolution (eg, $10 \times 10 \times 10$ mm in the Pirzkall study, compared with a resolution of $2 \times 2 \times 5$ mm in our study). Because other imaging modalities provide different information on the pathologic features of tumors, it is likely that future studies will combine these modalities. For example, combining the information about white matter disruption from DTI with metabolic information derived from MR spectroscopy might allow us to better characterize the tumor infiltration and thus allow us to determine the best individual treatment for that patient.

Other published data have shown differences in the peritumoral brain using diffusion tensor imaging. Several groups have shown no difference in the apparent diffusion coefficient (ADC) values from the peritumoral area of high-grade gliomas versus either metastases or low-grade gliomas,²⁵⁻²⁷ though there appears to be a region with a lower ADC in the adjacent normal-appearing white matter in high-grade gliomas compared with low-grade.²⁸ Various studies using DTI have found no difference in FA measurements in the peritumoral tissue of high-grade gliomas compared with minimally or noninfiltrating tumors such as metastases or meningiomas²⁹⁻³¹ but have found differences in other parameters such as the visual appearance of the FA maps,³¹ mean diffusivity,²⁹ and the magnitude of the principal eigenvalues.³⁰ As can be seen from equation 1, FA can be altered by changes in either the anisotropic or isotropic components of the tensor. The insensitivity to changes seen after stroke lead to the suggestion

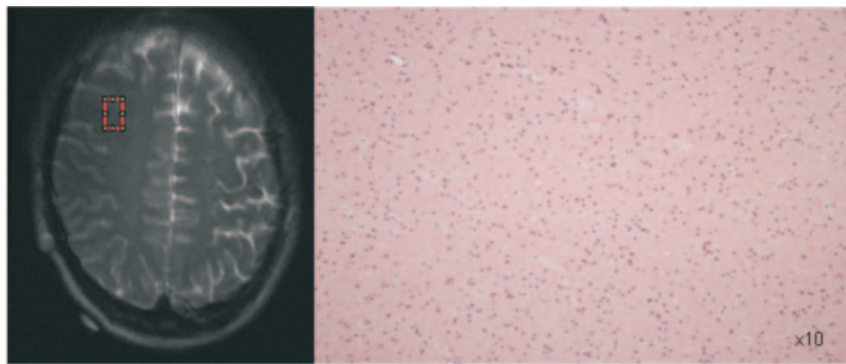


Fig 3. Biopsies taken from 3.5 cm from the target of the patient in Figure 1. Both MR and histology show that this is from normal brain. The tissue signatures from this region show that both the p value and q values are similar to control values.

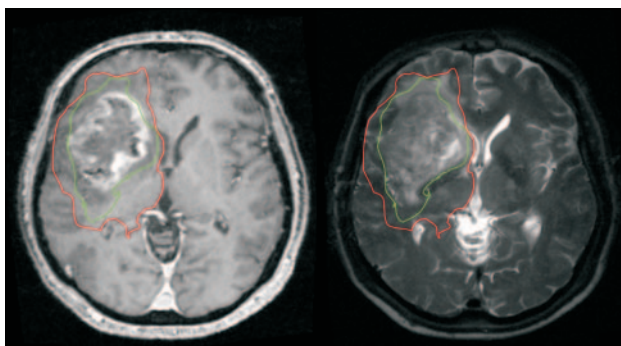
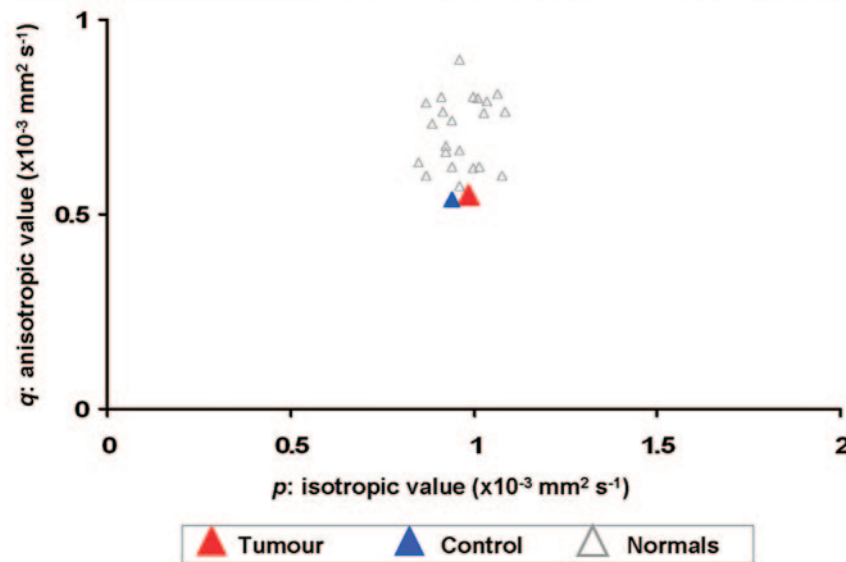


Fig 4. A gadolinium-enhanced T1-weighted (left) and T2-weighted (right) image from a 67-year-old man who presented with headaches and a left hemiparesis. Our results have shown that we can identify a region around a tumor with decreased anisotropy (q , shown in green) that shows the limit of the gross tumor, and a region around this with normal anisotropy but increased isotropy (p , shown in red) that can identify the infiltrating tumor margin. These zones extend beyond the abnormal areas on both enhanced T1- and T2-weighted MRI

of developing techniques used in engineering to better visualize changes in the diffusion tensor.³²

One other study has attempted to use diffusion techniques to correlate with histologic appearances to identify tumor margin.³³ In that study, 2-mm image-guided biopsies were taken from 22 patients with a variety of gliomas and compared with ADC values. No significant difference was found between the ADC of tumor and the peritumoral tissue, defined as showing reactive gliosis without tumor cells. The ADC values from all tumors were grouped, though a number of different

grades were present, all of which have different ADC values. We have avoided using mean values, preferring the minimum threshold that can differentiate tumor from normal tissue.

It is well recognized that the usage of steroids can alter diffusion parameters.³⁴ In this study, all patients with high-grade gliomas and 3 patients with low-grade gliomas were treated with dexamethasone. In such a study, we feel it would be unethical to withdraw steroids in this group of patients. Sinha et al³⁴ showed that dexamethasone affects only diffusion within the tumor and not in the normal brain. In their study, the reduction of mean diffusivity (essentially p) was approximately 7% in the peritumoral tissue of high-grade gliomas; there was no change in the FA values. We would expect no change, therefore, in the anisotropic component (q), but we would expect a reduction of p . In other words, although steroids might lead to an *underestimation* of the size of the infiltrated brain, we have seen no evidence of this.

Another potential limitation of our study is the use of image coregistration of echo-planar data with the distortions that accompany them, to non-echo-planar SPGR images. All image-guided biopsies were planned using the SPGR images. The sequence used exceeds the minimum specification from the navigation system. Using vtkCSIG allows the echo-planar image to be registered using both an affine and nonrigid body transformation. The positions of anatomic ROIs were compared after registration and were shown to match closely. All regions had an agreement within 1 mm. Patients with tumors in areas where there is usually much distortion (ie, above frontal air sinuses or petrous bone) were excluded.

Because the DTI technique is sensitive to changes in white matter architecture as well as changes in edema and cellularity, it cannot differentiate between infiltration of tumor or inflammatory cells. It will also be unable to identify isolated tumor cells that we know can be found some distance from the main tumor.^{13,35} Reviewing our histologic specimens would suggest that any isolated tumor cells would only be present in low numbers. These should be successfully sterilized by current treatments, which is consistent with the observation that virtually all gliomas recur within the high-dose treatment volume and not from the peripheral isolated tumor cells.^{2,3}

Incorporating DTI data into treatment planning will be an important development for existing and novel treatment strategies, to optimize their value. For example, it may allow more precise tumor-directed surgical resection, to achieve maximum safe tumor cytoreduction. DTI can now be incor-

porated into radiation therapy planning, allowing individualization of clinical target volume margins.³⁶ In particular, the volume of normal brain irradiated at a high dose can be reduced, and patients most likely to benefit from dose-escalation can be identified. Combined with intensity-modulated radiation therapy (IMRT), which allows better “sculpting” of radiation therapy dose, this should permit dose escalation without additional risk of radiation damage. In combination with other imaging techniques (for example MR spectroscopy), DTI will be an important component of “biologic targeting” for radiation therapy.

There is currently great interest in developing novel local therapies to improve outcome in gliomas. These include existing drugs, receptor-targeted toxins, cell signaling blocking agents, and gene therapies. At present, these therapies are administered indiscriminately to all parts of the resection cavity, whether using polymer wafers (eg, Gliadel wafers [MGI Pharma, Bloomington, Minn]), injectable bio-polymers (eg, 5-fluorouracil polymers), by direct inoculation (eg, most gene therapy studies), or by convection-enhanced delivery. Imaging techniques that allow specific targeting to areas of greatest tumor infiltration or burden are likely to enhance the efficacy of these new modalities.

By imaging areas of tumor infiltration, DTI will improve the correlation between clinical behavior and tumor pathology, particularly gene expression. DTI-targeted stereotactic biopsies would allow precise sampling from areas of infiltrating tumor.

Through its ability to detect infiltration, DTI may allow triage of patients between aggressive therapy, standard treatment, or supportive management, and for those persons likely to benefit from aggressive treatment, it should guide the choice of multitechnique management.

Conclusion

This study has shown that the use of diffusion tissue signatures can delineate the margin of gliomas better than conventional imaging and can differentiate regions of gross tumor from regions of tumor infiltration. Such a technique could contribute to targeting specific treatment modalities to the sites of greatest tumor burden and by guiding the optimal combination of treatment options in an individual patient.

References

- Walker MD, Alexander E Jr, Hunt WE, et al. Evaluation of BCNU and/or radiotherapy in the treatment of anaplastic gliomas. A cooperative clinical trial. *J Neurosurg* 1978;49:333–43
- Oppitz U, Maessen D, Zunterer H, et al. 3D-recurrence-patterns of glioblastomas after CT-planned postoperative irradiation. *Radiother Oncol* 1999;53:53–57
- Chan JL, Lee SW, Fraass BA, et al. Survival and failure patterns of high-grade gliomas after three-dimensional conformal radiotherapy. *J Clin Oncol* 2002;20:1635–42
- Fitzek MM, Thornton AF, Rabinov JD, et al. Accelerated fractionated proton/ photon irradiation to 90 cobalt gray equivalent for glioblastoma multiforme: results of a phase II prospective trial. *J Neurosurg* 1999;91:251–60
- Daumas-Duport C, Meder JF, Monsaingeon V, et al. Cerebral gliomas: malignancy, limits and spatial configuration. Comparative data from serial stereotaxic biopsies and computed tomography (a preliminary study based on 50 cases). *J Neuroradiol* 1983;10:51–80
- Scherer HJ. The forms of growth in gliomas and their practical significance. *Brain* 1940;63:1–35
- Lilja A, Bergstrom K, Spannare B, et al. Reliability of computed tomography in assessing histopathological features of malignant supratentorial gliomas. *J Comput Assist Tomogr* 1981;5:625–36
- Selker RG, Mendelow H, Walker M, et al. Pathological correlation of CT ring in recurrent, previously treated gliomas. *Surg Neurol* 1982;17:251–54
- Burger PC, Dubois PJ, Schold SC Jr, et al. Computerized tomographic and pathological studies of the untreated, quiescent, and recurrent glioblastoma multiforme. *J Neurosurg* 1983;58:159–69
- Burger PC, Heinz ER, Shibata T, et al. Topographic anatomy and CT correlations in the untreated glioblastoma multiforme. *J Neurosurg* 1988;68:698–704
- Lunsford LD, Martinez AJ, Latchaw RE. Magnetic resonance imaging does not define tumor boundaries. *Acta Radiol Suppl* 1986;369:154–56
- Kelly PJ, Daumas-Duport C, Kispert DB, et al. Imaging-based stereotaxic serial biopsies in untreated intracranial glial neoplasms. *J Neurosurg* 1987;66:865–74
- Watanabe M, Tanaka R, Takeda N. Magnetic resonance imaging and histopathology of cerebral gliomas. *Neuroradiology* 1992;34:463–69
- Le Bihan D, Turner R, Douek P. Is water diffusion restricted in human brain white matter? An echo-planar NMR imaging study. *Neuroreport* 1993;4:887–90
- Price SJ, Burnet NG, Donovan T, et al. Diffusion tensor imaging of brain tumours at 3T: a potential tool for assessing white matter tract invasion? *Clin Radiol* 2003;58:455–62
- Provenzale JM, McGraw P, Mhatre P, et al. Peritumoral brain regions in gliomas and meningiomas: investigation with isotropic diffusion-weighted MR imaging and diffusion-tensor MR imaging. *Radiology* 2004;232:451–60
- Price SJ, Pena A, Burnet NG, et al. Detecting glioma invasion of the corpus callosum using diffusion tensor imaging: a case report. *Br J Neurosurg* 2004;18:391–95
- Donovan T, Fryer TD, Pena A, et al. Stereotactic MR imaging for planning neural transplantation: a reliable technique at 3 Tesla? *Br J Neurosurg* 2003;17:443–49
- Basser PJ, Mattiello J, LeBihan D. Estimation of the effective self-diffusion tensor from the NMR spin echo. *J Magn Reson B* 103:247–54, 1994
- Price SJ, Pena A, Burnet NG, et al. Tissue signature characterisation of diffusion tensor abnormalities in cerebral gliomas. *Eur Radiol* 2004;14:1909–17
- Studholme C, Hill DL, Hawkes DJ. Automated three-dimensional registration of magnetic resonance and positron emission tomography brain images by multiresolution optimization of voxel similarity measures. *Med Phys* 1997;24:25–35
- Pirzkall A, Li X, Oh J, et al. 3D MRSI for resected high-grade gliomas before RT: tumor extent according to metabolic activity in relation to MRI. *Int J Radiat Oncol Biol Phys* 2004;59:126–37
- McKnight TR, dem Bussche MH, Vigneron DB, et al. Histopathological validation of a three-dimensional magnetic resonance spectroscopy index as a predictor of tumor presence. *J Neurosurg* 2002;97:794–02
- Croteau D, Scarpace L, Hearshen D, et al. Correlation between magnetic resonance spectroscopy imaging and image-guided biopsies: semiquantitative and qualitative histopathological analyses of patients with untreated glioma. *Neurosurgery* 2001;49:823–29
- Kono K, Inoue Y, Nakayama K, et al. The role of diffusion-weighted imaging in patients with brain tumors. *AJNR Am J Neuroradiol* 2001;22:1081–88
- Stadnik TW, Chaskis C, Michotte A, et al. Diffusion-weighted MR imaging of intracerebral masses: comparison with conventional MR imaging and histologic findings. *AJNR Am J Neuroradiol* 2001;22:969–76
- Lam WW, Poon WS, Metreweli C. Diffusion MR imaging in glioma: does it have any role in the pre-operation determination of grading of glioma? *Clin Radiol* 2002;57:219–25
- Bulakbasi N, Kocaoglu M, Ors F, et al. Combination of single-voxel proton MR spectroscopy and apparent diffusion coefficient calculation in the evaluation of common brain tumors. *AJNR Am J Neuroradiol* 2003;24:225–33
- Lu S, Ahn D, Johnson G, et al. Peritumoral diffusion tensor imaging of high-grade gliomas and metastatic brain tumors. *AJNR Am J Neuroradiol* 2003;24:937–41
- Wiegell MR, Henson JW, Tuch DS, et al. Diffusion tensor imaging shows potential to differentiate infiltrating from non-infiltrating tumors. *Proc Intl Soc Mag Reson Med* 2003;11:2075
- Tsuchiya K, Fujikawa A, Nakajima M, et al. Differentiation between solitary brain metastasis and high-grade glioma by diffusion tensor imaging. *Br J Radiology* 2005;78:533–37
- Green HA, Pena A, Price CJ, et al. Increased anisotropy in acute stroke: a possible explanation. *Stroke* 2002;33:1517–21
- Pauleit D, Langen KJ, Floeth F, et al. Can the apparent diffusion coefficient be used as a noninvasive parameter to distinguish tumor tissue from peritumoral tissue in cerebral gliomas? *J Magn Reson Imaging* 2004;20:758–64
- Sinha S, Bastin ME, Wardlaw JM, et al. Effects of dexamethasone on peritumoral oedematous brain: a DT-MRI study. *J Neurol Neurosurg Psychiatry* 2004;75:1632–35
- Silbergeld DL, Chicoine MR. Isolation and characterization of human malignant glioma cells from histologically normal brain. *J Neurosurg* 1997;86:525–31
- Jena R, Price SJ, Baker C, et al. Diffusion tensor imaging: possible implications for radiotherapy treatment planning of patients with high-grade glioma. *Clin Oncol* 2005;17:581–90